Automated surface inspection of friction stir welds by means of structured light projection

IOP Conf. Series: Materials Science and Engineering 480 (2019) 012035 doi:10.1088/1757-899X/480/1/012035

Automated surface inspection of friction stir welds by means of structured light projection

R Hartl*, A Bachmann, S Liebl, A Zens and M F Zaeh

Institute for Machine Tools and Industrial Management, Technical University of Munich, Boltzmannstrasse 15, 85748 Garching, Germany

* e-mail: roman.hartl@iwb.mw.tum.de

Abstract. Friction stir welding is an innovative joining technology that is particularly suitable for aluminium alloys. Various studies have shown a significant dependence of the weld seam quality on the welding speed and the rotational speed of the tool. Frequently, an unsuitable setting of these parameters can be detected by visual examination of resulting surface defects, such as increased flash formation, surface galling, or irregular formation of the surface arc texture. The visual inspection for these defects is often conducted manually and is therefore associated with increased costs and personnel effort. In this work, a method to automatically detect irregularities and features on the weld surface is introduced. It is based on a three-dimensional shape detection of the surface features using structured light projection. For this purpose, the topography of EN AW-5754-H111 sheets, welded in a butt joint configuration, was measured. The data were evaluated and characteristic key structures of the weld seam surface were derived. It was shown that welding irregularities can be detected automatically by an evaluation of the weld seam topography. The results are the basis for the future development of an inline quality monitoring and parameter control method for friction stir welding.

1. Introduction

The annual primary aluminium production has increased from 19.1 million tonnes in 1994 to 60 million tonnes in 2017 [1]. The main reasons for this trend are the versatile applications and the properties of aluminium alloys, such as the high specific strength compared to other metals [2]. The increasing demand of aluminium alloys in the industry also increases the need for suitable processes to join aluminium components. Friction stir welding (FSW) is a solid state welding process, which makes it very suitable for materials that are difficult or impossible to weld by fusion welding processes due to problems with the formation of brittle phases, gas pores and cracking [3]. Hence, friction stir welding has already found applications in various sectors of industry. A popular example are the friction-stir-welded tailored blanks, which are subsequently deep-formed to make the center closing panel of the Audi R8 [4]. KAHNERT ET AL. [5] describe the use of FSW for launcher systems at MT Aerospace.

The weld quality in friction stir welding is affected by various characteristic defects produced during the welding process [6]. The DIN EN ISO 25239-5 standard [7] provides an overview of the different types of defects that can occur at FSW of aluminium and its alloys. The standard enumerates seven surface irregularities and two internal irregularities. The mentioned surface irregularities are: incomplete penetration (also known as lack of penetration, LOP), excessive root elevation, excessive flash formation, edge offset, seam underfill, irregular seam width, and irregular seam surface. The

standard also specifies admissible acceptance criteria for some surface defects. For example, the calculation rule for the permissible seam underfill h for sheets with a minimum thickness t of 2 mm is:

$$h \leq 2\ \text{mm} + 0.1 \cdot t\,. \tag{1}$$

In accordance with DIN EN ISO 25239-5 [7], the surface defects listed therein can be detected by visual inspection, with the exception of insufficient penetration welding. As per DIN EN ISO 25239-4 [8], a 100 % visual inspection of finished friction stir welds is mandatory in order to meet the requirements for the qualification of a welding process for friction stir welding of aluminium. The tunnel defect as well as internal deformations are regarded as internal irregularities according to the standard [7].

ZETTLER ET AL. [9] divided the causes of seam defects at friction stir welding into defects from welding at excessively high temperatures, defects from welding at too low temperatures, and defects caused by geometrical mistakes. Flaws that are generated under too high processing temperatures are visually identifiable through the surface appearance of the welded joint. In extreme cases, the surface appears to contain blisters or surface galling. In addition, distinct heat generation can lead to excessive surface flash formation. Visually discernable flaw types as a result of welding at too low temperatures are a surface lack of fill (surface LOF) and tunnel defects. Tunnel defects can easily be confirmed by inspecting the exit hole left after the retraction of the tool probe from the workpiece. Thus, most flaw types that develop due to welding at too cold conditions produce coarse and visually identifiable flaws [10]. Defects from geometrical mistakes include a gap between the workpieces, a thickness mismatch, or a plate thickness variation.

SINHA ET AL. [11] report the possibility to automatically detect surface defects of friction stir welds by means of image data processing with the aim of gathering information about the seam quality. The images of the FSW seams were captured by a camera tracking the weld behind the tool and then processed offline, for example by histogram equalization, contrast stretching, and various filtering techniques. For sound welds, the processed images showed a low variation in the pixel intensities along a selected line in the contouring data. However, the contour plot as well as the grey values along an evaluated line showed larger variations when a probe failure occurred. The authors also noted that an online monitoring system can improve the productivity and quality of the friction stir welding process. They propose a system that uses a camera to record images of the seam, which are then processed using algorithms to detect any defects on the surface. In addition, the suggested online system can estimate the appropriate process parameters for new materials. RANJAN ET AL. [12] describe the automated detection and classification of various surface imperfections resulting from FSW using digital image processing. The localization and expression of the severity of the defects are evaluated individually for each defect type by intensity plots along the weld seam. In order to recognize the defects in the pictures more easily, grey value filters, median filters, Hough transform, image pyramid based processing techniques, and other methods were used. RANJAN ET AL. [12] also express the use of their gained knowledge for online monitoring. The calculation time to run the MATLAB code is given as approximately 3.9 seconds for one frame. This enables an online adaption of the welding parameters. The computer architecture used is not specified.

DENG ET AL. [13] have investigated the influence of the welding speed v_s and the rotational speed n of the tool on the surface topography of the friction stir weld. On the one hand, the authors found that there is a linear relationship between the input parameters and the distance between the individual arc textures on the surface. If, on the other hand, the ratio between the rotational speed n and the welding speed v_s remains constant, the distance between the arc lines on the surface is the same. ZUO ET AL. [14] also investigated the influence of process parameters on the surface topography of friction stir welds. According to the authors, the surface topography plays an important role in the quality of the joint. Another finding was that the distance between the arc lines on the surface decreases with increasing rotational speed n or decreasing welding speed v_s. However, the depth of the surface arc texture was independent of the input variable magnitudes.

The cited works on the automated analysis of the seam surface at FSW are based either on the detection of defects through image data or on the influence of process parameters on the topography of the weld seam. For the detection of defects based on image data, a series of image processing steps is necessary. The detection of defects based on the weld topography has not yet been investigated.

In the context of this work, it was studied how surface defects of friction stir welds can be detected and quantified by evaluating the three-dimensional point cloud obtained by structured light projection.

2. Hypothesis and methodology

2.1. Hypothesis

Previous work has shown that the welding speed v_s and the rotational speed n of the tool have a significant influence on the surface and thus on the topography of the friction stir weld. An unsuitable setting of these input parameters often leads to weld seam surface defects.

The hypothesis is that it is possible to derive one-dimensional characteristic structures from the three-dimensional point cloud representing the surface topography, which allow an automated identification and quantification of surface features. This would be an extension of the existing approaches and a step towards a fully automated surface inspection during friction stir welding.

2.2. Approach

First, a sufficient parameter window was defined for the welding tests. Both the welding speed v_s and the rotational speed n were varied in a large parameter window in order to produce welds with different surface defects as well as welds without surface irregularities. Two studies, labelled study 1 and study 2, were conducted in order to prove the hypothesis posed in section 2.1. In both studies, the aluminium alloy EN AW-5754-H111 was used. The welds in study 1 (experiments 1 to 16) were produced with a concave shoulder geometry, whereas in study 2 (experiment 17 to 32) a flat shoulder with a spiral contour was employed. After welding, the generated seams were first inspected visually and the obtained surface defects were determined. The weld surface was then recorded by means of structured light projection. The produced three-dimensional point cloud was further processed in order to generate one-dimensional key indicators, which were intended to quantify the investigated quality of the surface.

2.3. Experimental set-up

2.3.1. Welding experiments. The welding machine used during the studies was a 4-axis horizontal milling machine MCH 250 from Gebr. Heller Maschinenfabrik GmbH, which had been adapted to perform friction stir welding. The maximum axial force of the system was 30 kN. Two-piece tools consisting of a shoulder and a conical welding probe with an M6 thread and three flats were used for the two studies. The tool geometry for study 1 is given in figure 1. The tool for study 2 was identical with the exception of the shoulder contour. Table 1 lists the most important dimensions for both tools.

Welds with a length of 150 mm were made on 4 mm thick plates of EN AW 5754 H111. The plates were fixed on a backing made of unalloyed tool steel. In both studies, the welding speed vs and the rotational speed n were systematically varied.

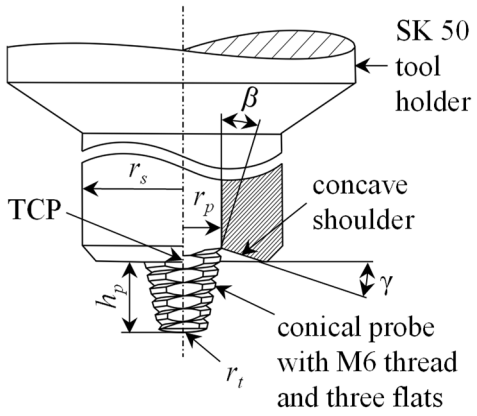

Figure 1. Tool geometry for study 1 with the most important dimensions (adapted from BACHMANN ET AL. [15]).

Table 1. Dimensions for the used tools.

Tool type 1 and 2	
Probe radius r_p	3 mm
Shoulder radius r_s	7 mm
Conical probe angle β	10°
Probe length h_p	3.85 mm
Probe tip radius r_t	10 mm
Tool type 1	
Concave shoulder angle γ	10 °
Tool type 2	
Width of the spirals	0.7 mm
Depth of the spirals	0.7 mm
Spiral angle	360 °
Spiral mean start radius	3 mm
Spiral mean end radius	6 mm

The tilt angle of the tool was kept constant at 2° and the dwell time at start of weld was 1 second in all experiments. The plunge depth of the Tool Center Point (TCP) was 0.1 mm throughout the experiments. The geometry of the samples is shown in figure 2. The specimens were dimensioned with a length of 342 mm and a width of 88 mm. A rigid clamping device avoided gaps between the joining partners. To reduce the experimental effort, two 150 mm long welds were made on each sheet configuration.

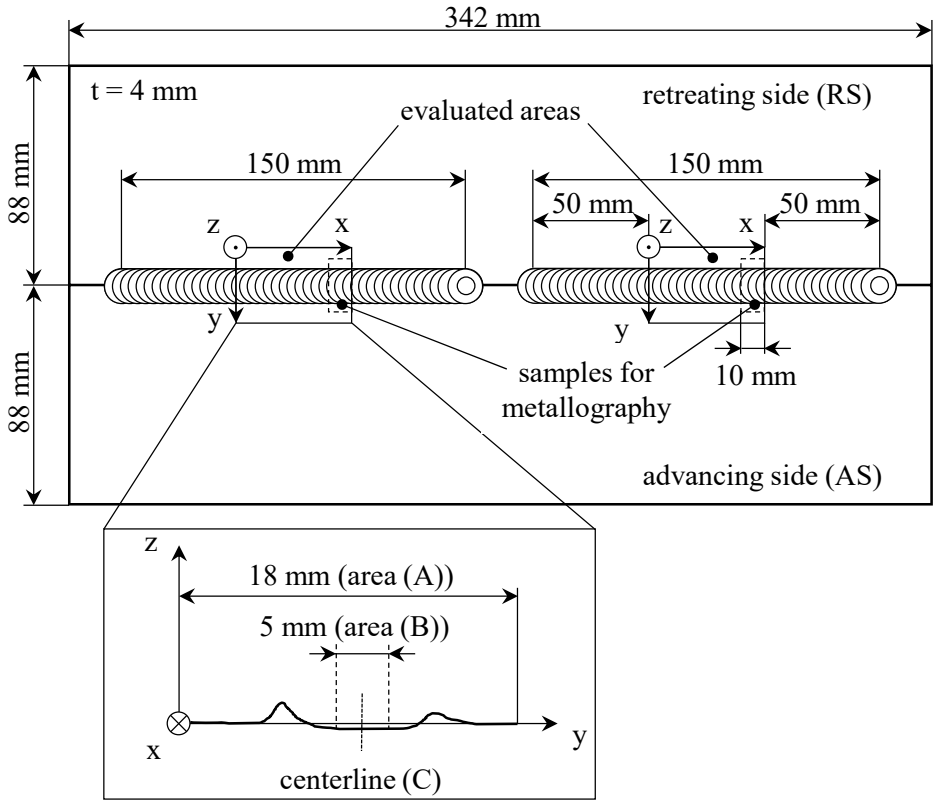

Figure 2. Dimensions of the welded plates and positions of the evaluated surface areas.

The investigated parameter window is depicted in figure 3 and was adapted from ZAEH ET AL. [16]. In figure 3, the tested parameter sets are marked as circles and labelled with the experiment numbers for study 1 and study 2 as well as the ratio n/v_s between the rotational speed n and the welding speed v_s, respectively. In order to protect the welding equipment, the minimum n/v_s ratio was limited to 1 mm^{-1}. The welding speed v_s and the rotational speed n were varied in four equidistant steps, respectively. This resulted in a full factorial experimental plan with 16 welds each for study 1 and study 2.

2.3.2. Visual inspection. After welding, the seams were inspected visually. Particular attention was paid to surface defects such as flash formation, surface galling and irregular formation of the surface texture. Additionally, the plunge site and the exit hole were inspected. Often, welding irregularities can already be noticed at the plunge point. Tunnel defects can be detected via the exit hole.

2.3.3. Topography analysis. After the visual inspection, the topography of the welds was examined using a three-dimensional profilometer VR-3100 from KEYENCE DEUTSCHLAND GmbH based on phase-coded structured light projection. The white LEDs projected light from two places onto the welds with an angle of incidence of 35°. The reflected light was measured by a CMOS sensor. The resolution of the height measurement (z axis) was 0.1 µm. The smallest measurable difference in the z-direction was 1 µm. The distance between the individual topography points in the width (x-y plane) was 23.549 µm. The measurement accuracy was 3 µm in the height and 5 µm in the width. The repeatability was 0.5 µm in the height and 1 µm in the width. A 12-fold magnification was used, resulting in a viewing measurement range of 24 mm x 18 mm for each frame. The first 50 millimeters as well as the last 50 millimeters of the welds were not used for evaluation, as the welding conditions may not have been stationary there. This resulted in a 50 mm long seam section that was used for the evaluation of the surface. To enable an evaluation of the 50 mm long weld piece, at least two single frames had to be stitched. Depending on whether the topography of the entire seam, a section of the inner seam surface, or along a single line should be evaluated, either the area (A) or (B), or the centerline (C) was investigated (see figure 2). The zero height was always referenced to the sheet surface. Additionally, existing inclinations of the sheet metal were averaged out. These can occur due to sheet unevenness or distortion during welding. As the distance between the individual topography points in the x-y plane was 23.549 µm, this led to 2123 height information points along the welding direction. The weld seam width on the surface was approximately 14 mm as the shoulder diameter was 14 mm. This resulted in 594 height information points over the weld width. Thus, approximately 1.26 million topography points were evaluated in total per weld seam.

2.3.4. Metallography. Metallographic examinations were conducted on individual welds in order to investigate the weld surface more closely. Both, cross sections and longitudinal sections, were produced for this purpose. The samples were taken from the sheets with the aid of a wet cut-off grinder. The positions at which the metallographic samples were taken are labelled in figure 2. The samples were embedded in epoxy resin to stabilize the surface characteristics created during welding and to prevent damage during grinding and polishing. The embedded samples were first surface ground with P320 silicon carbide wet abrasive paper according to the FEPA P grit standard [17] and then finish-ground with P1000 silicon carbide wet abrasive paper, also according to the FEPA P grit standard. Finally, the cuts were micro-etched according to Kroll [18]. The cross sections were recorded with the three-dimensional profile measuring device VR-3100 from KEYENCE DEUTSCHLAND GmbH. Thereby the image mode of the profilometer was used. The longitudinal sections were analyzed with the Nikon MM-40 Measuring Microscope.

3. Results and discussion

3.1. Visual surface inspection

The most important surface defects detected during the visual inspection are indicated in figure 3 by differently coloured rings.

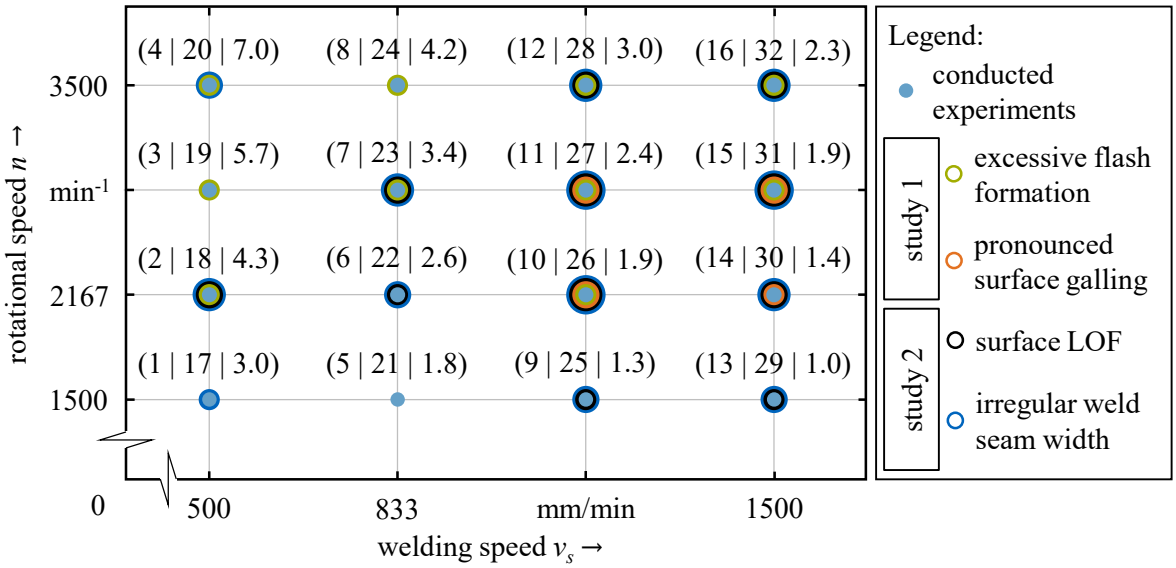

Figure 3. Experimental plan with numbering (experiment no. for study 1 | experiment no. for study 2 | n/v_s ratio in mm^{-1}) and surface defects (evaluated by visual inspection) noted for each point within the process window.

The visual examination of the experiments from study 1 (tool type 1) led to the following results:

- The most notable surface defects were the occurrence of increased flash formation and surface galling.
- The best welding result by means of the visual inspection was achieved in experiment no. 1 with v_s 500 mm/min and n 1500 mm/min. In this experiment, the flash formation on both the advancing side and the retreating side was very low and uniform. Excessive surface galling or an irregular surface arc texture could not be detected. Furthermore, the weld seam width was very uniform.
- The flash formation was more pronounced on the retreating side than on the advancing side in all experiments conducted in study 1.
- At n/v_s ratios smaller than 3 mm^{-1}, the flash formation was more irregular and was chip- or fringe-shaped. If the n/v_s ratio was at least 3 mm^{-1}, the flash formation was more continuous and wave-like.
- Surface galling was noticeably detectable in the experiments no. 10, 11, 14, and 15 (see figure 3). Within the examined parameter window, these tests were performed with a high welding speed v_s and a medium rotational speed n.
- During the inspection of the exit hole a tunnel defect was not detected in any of the welds.

The visual examination of the experiments from study 2 (tool type 2) revealed the following results:

- The most notable surface defects were the surface lack of fill (surface LOF) as well as a very irregular weld seam width.
- Based on the visual inspection, the best welding results in study 2 were obtained in experiments no. 19 and 20.
- The surface lack of fill appeared as a crack or seam collapse on the surface, so that the seam surface was not closed (all experiments except no. 17, 19, 20, 21, and 24).

- An irregular weld seam width occurred in almost all experiments with tool type 2. Only in the experiments no. 19, 21, and 24 the weld width was evaluated as regular on the basis of the visual inspection.

Thus, when using the concave tool shoulder (study 1), excessive flash formation and pronounced surface galling occurred and when using the spiral tool shoulder (study 2), the surface lack of fill and an irregular weld seam width were the primary surface defects. The annotated surface defects were therefore specific to the used tool shoulder geometry.

3.2. Topography analysis

The topography of the weld seams was investigated with the aim of deriving one-dimensional characteristic structures from the three-dimensional point cloud. The key structures are intended to enable an automated detection of surface defects and features, and thus mirror the visual inspection of the seam surface. Based on the results of the visual inspection, in study 1 the flash formation, the occurrence of surface galling and the regularity of the surface texture were examined through the structured light projection. In contrast, the weld seams from study 2 were investigated with regard to the surface lack of fill and an irregular weld seam width.

3.2.1. Flash formation. Since the flash formation was more pronounced on the retreating side than on the advancing side in all experiments from study 1, only the retreating side was used to evaluate the flash formation. Over a weld seam length of 50 mm (area (A) in figure 2), the complete flash volume f_{Vol}, the maximum flash height f_{max}, and the standard deviation of the flash height S_f were determined. As described in section 2.3.3, a height of zero corresponded to the position of the sheet surface.

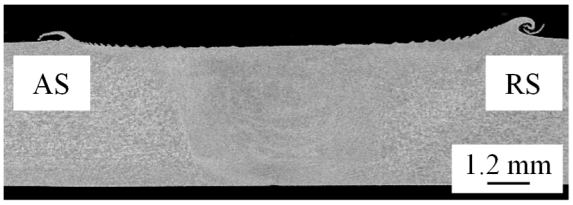

Figure 4. Cross section of the weld from experiment no. 1 with clearly visible cavities under the formed flash.

When determining the flash volume f_{Vol} by means of structured light projection, it was disadvantageous that in some evaluated experiments cavities below the flash were included in the measurement (see figure 4). This led to measurement errors that could not be avoided. The flash volume f_{Vol} was therefore not suitable to evaluate the flash formation. The cross section in figure 4 was prepared as described in section 2.3.4. Figure 5 displays the maximum flash height f_{max} as well as the standard deviation of the flash height S_f on the retreating side for the 16 experiments conducted in study 1. In experiment no. 1 the maximum flash height f_{max} was 0.708 mm and the standard deviation of the flash height S_f was 0.016 mm. This were the lowest values out of all experiments conducted in study 1, which was consistent with the finding that experiment no. 1 was the best welding result in study 1 by means of the visual examination (see section 3.1). The lower the flash height and the more even the flash formation, the better the result of the visual inspection of the weld surface was in terms of the flash formation. The maximum flash height f_{max} and the standard deviation of the flash height S_f therefore appear to be the most suitable key-indicators to evaluate the flash formation of friction stir welds by means of the surface topography.

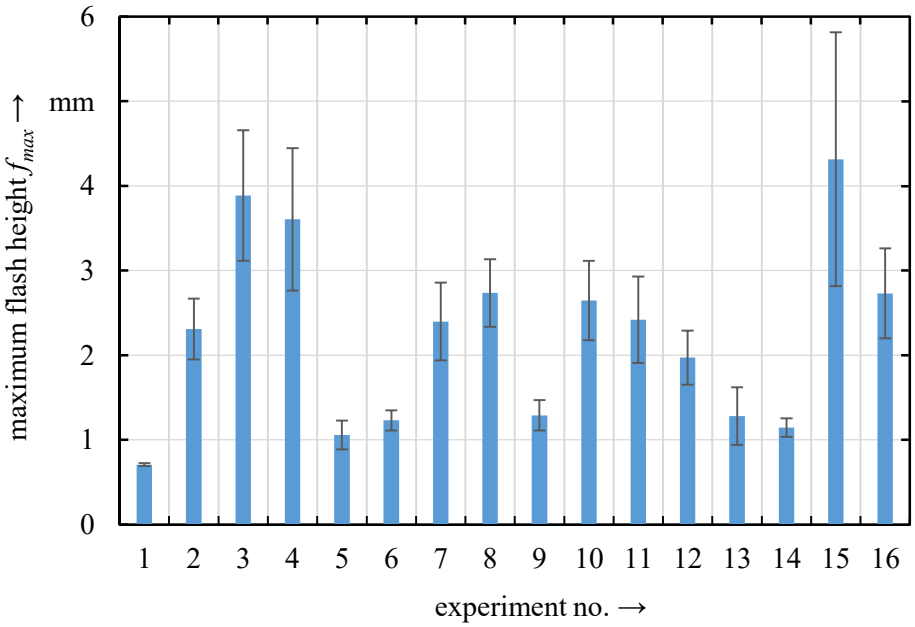

Figure 5. Maximum flash height (f_{max}) and the standard deviation of the flash height (S_f).

3.2.2. Surface galling. Another surface defect, which was found during the visual inspection, is surface galling. Surface galling on friction stir welds is embodied by material particles that either deposit loosely on the surface of the weld seam or protrude from the weld surface. To the best of the authors' knowledge, no procedure to quantitatively evaluate the occurrence of surface galling has been described in literature to date. According to the visual examination, the experiment with the most pronounced surface galling in study 1 was experiment no. 10. Figure 6 depicts a comparison of longitudinal sections of experiment no. 1, in which no pronounced surface galling was visible in the visual examination, with experiment no. 10.. In the longitudinal section of experiment 10, the protruding material artifacts are clearly visible, whereas the surface in experiment 1 is very regular and without surface galling. The longitudinal sections in figure 6 were prepared and recorded as described in section 2.3.4.

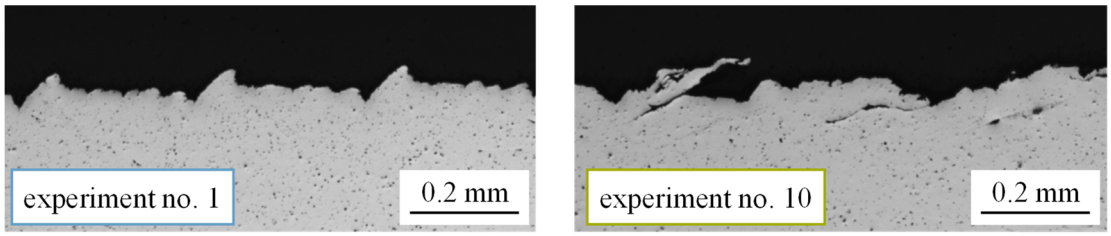

Figure 6. Longitudinal sections of the experiments no. 1 and 10.

Figure 7 (a) depicts an image and the elevation picture of the area (B) in top view for the experiments no. 1 and 10. The occurring surface galling in experiment no. 10 gets especially evident in the elevation picture. In particular the red areas with a height of approximately 0.2 mm above the sheet surface display strong surface galling.

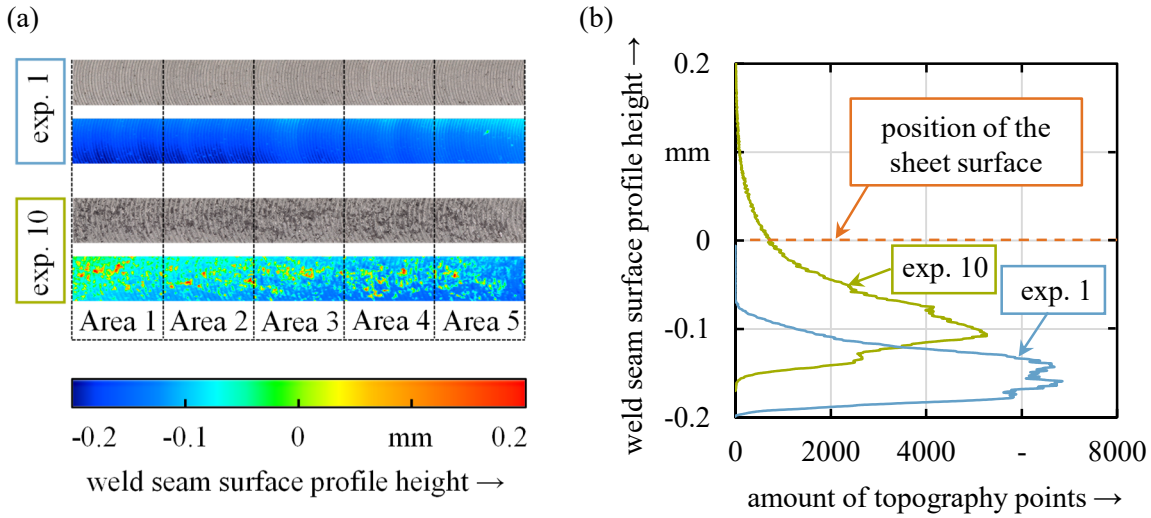

Figure 7. (a) Weld surface image and elevation picture of the experiments no. 1 and 10; (b) Distribution of the evaluated surface topography for experiment no. 1 and 10.

Since the surface galling in experiment no. 10 was easy to see from the elevation image in figure 7 (a), an attempt was made to use the height distribution of the topography points to find a way of quantifying surface galling. For that reason, the distributions of the topography points were compiled for the experiments no. 1 and 10 (see figure 7 (b)). In both experiments there were 450076 elevation points in area (B) (see figure 2), which was measuring 50 mm x 5 mm. Since the smallest measurable height difference, as specified in section 2.3.3, was 1 µm, the point cloud was discretized to 1 µm in the direction of the weld profile height (z-axis). Due to the seam underfill, most of the points were located below the sheet surface, which was adjusted at zero height (see section 2.3.3). Figure 7 (b) illustrates that the distribution of topography points in experiment no. 10 had a higher variance than in experiment no. 1. Additionally, the positive skewness of the distribution in experiment no. 10 was more pronounced than in experiment no. 1. This is visible through the longer tail of the distribution in the positive direction of the weld seam surface profile height in experiment no. 10 in figure 7 (b).

By accumulation and normalization of the height distribution of the surface profile, the material ratio curve (also known as Abbott-Firestone curve) results [19]. Figure 8 (a) shows a schematic representation of the material ratio curve. The figure also illustrates the peak material volume V_{mp}, the core material volume V_{mc}, the core void volume V_{vc}, and the dale void volume V_{vv}, according to the DIN EN ISO 25178-2 standard [20]. The peak material volume V_{mp} is defined as the area-related volume at a given material content p. The value for p can be taken from the ISO 25178-3 standard [21] and is 10 %. Due to the greater positive skewness of the height distribution of the topography points (see figure 7 (b)), it was assumed that the peak material volume V_{mp} gets increased by pronounced surface galling. This hypothesis is reinforced by figure 8 (b). There the material ratio curves are displayed for the experiments no. 1 and 10 for area (B). The colored filled areas below the material ratio curve with a material ratio that is smaller than p (10 %) mark the peak material volume V_{mp}. This area is larger in experiment no. 10, which reveals the larger V_{mp} compared to experiment no. 1.

The mean peak material volume as well as the standard deviation of the peak material volume for the areas 1 to 5 (see figure 7 (a)), each measuring 10 mm x 5 mm, were determined. The result is charted in figure 9.

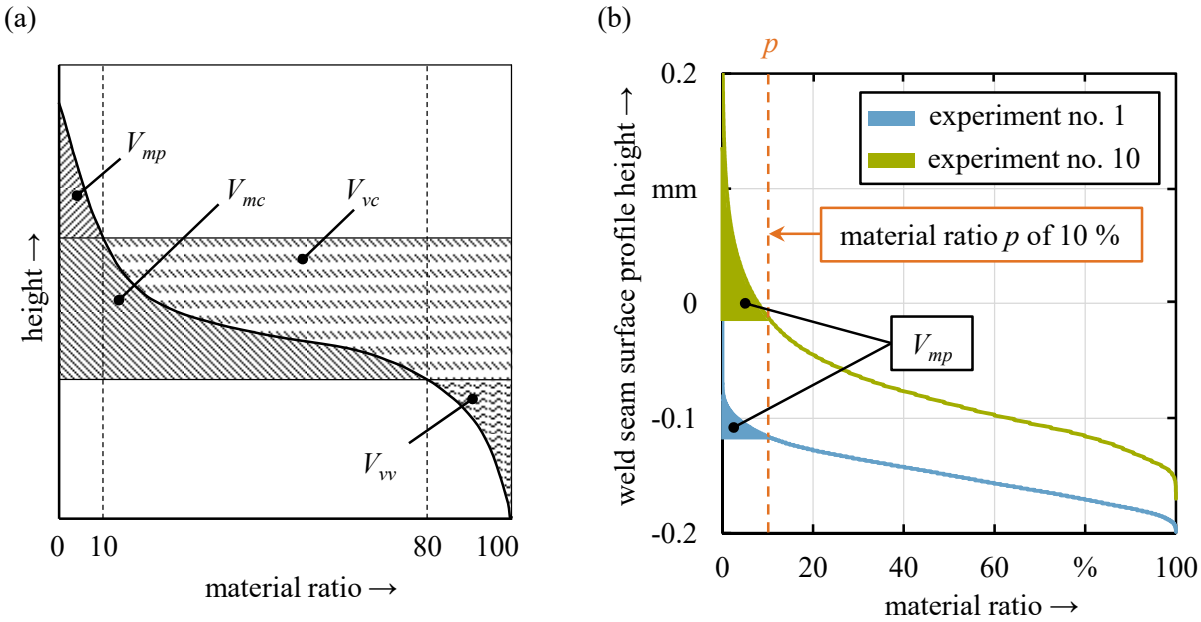

Figure 8. (a) Schematic representation of the parameters for the void volume (V_{vc}, V_{vv}) and the material volume (V_{mc}, V_{mp}); (b) Material ratio curves for the experiments no. 1 and 10.

Experiment no. 10, which revealed the largest amount of surface galling in the visual examination, also had the highest peak material volume V_{mp} out of all experiments in study 1. Experiment no. 1, which showed the best welding result in study 1 in terms of the visual examination, showed a low area-related peak material volume V_{mp} of 1.02 ml/m². In total, the evaluation of the peak material volume V_{mp} resulted in a good agreement with the detected surface galling by means of the visual inspection. When more surface galling occurred, higher amounts of peak material volume V_{mp} were measured. The peak material volume V_{mp} can therefore be used to detect and quantify occurring surface galling.

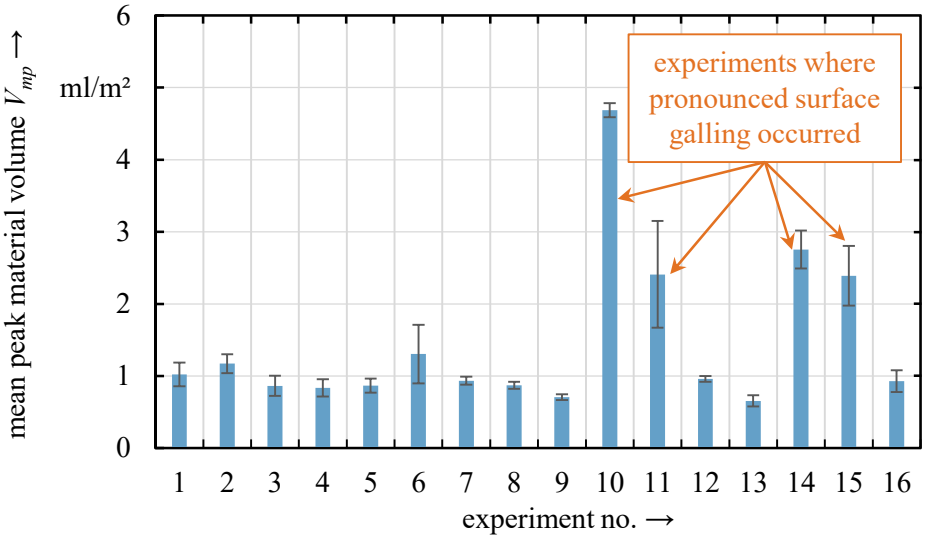

Figure 9. Mean peak material volume and standard deviation of V_{mp} for area (B).

3.2.3. Irregular arc texture formation. A further quality feature in the visual inspection of FSW seams is the regular formation of the arc texture on the weld surface. The periodicity of the surface arc

texture depends on the welding speed v_s and the rotational speed n of the tool. In contrast, the height difference in the texture is independent of both welding parameters [14]. The results of this study suggest that this is an idealization. Depending on the setting of v_s and n, irregularities occur on the weld surface, which influence the measured depth of the arc texture. For the evaluation of the surface, the arc texture along the centerline (C) (see figure 2) was examined. Figure 10 illustrates an excerpt of the evaluated arc texture of experiment no 1.

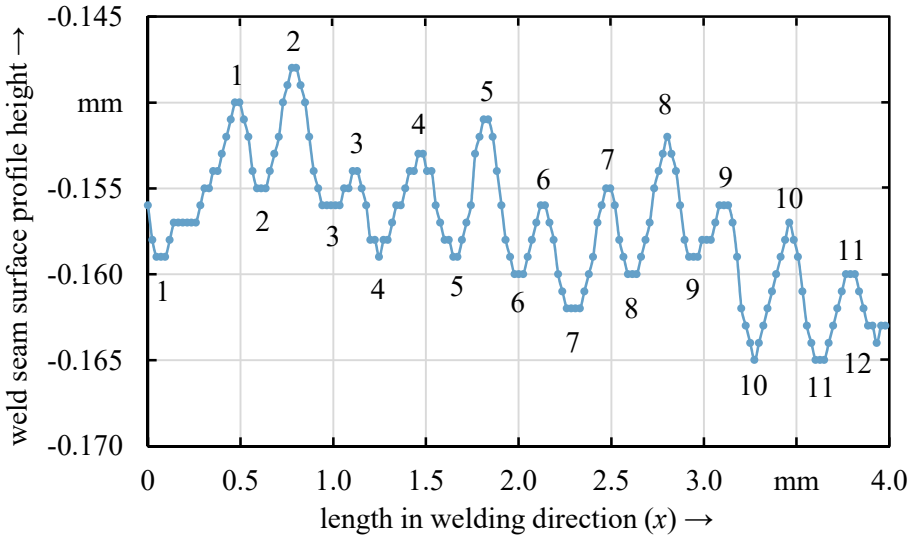

Figure 10. Weld seam arc texture for the first 4 mm of the evaluated centerline (C) (see figure 2) of experiment no. 1.

The calibration of 23.549 µm in the x-y plane mentioned in section 2.3.3 resulted in 170 measured points for the topography on the chosen 4 mm long section. The measured points of the topography are connected with linearly interpolated lines in figure 10.

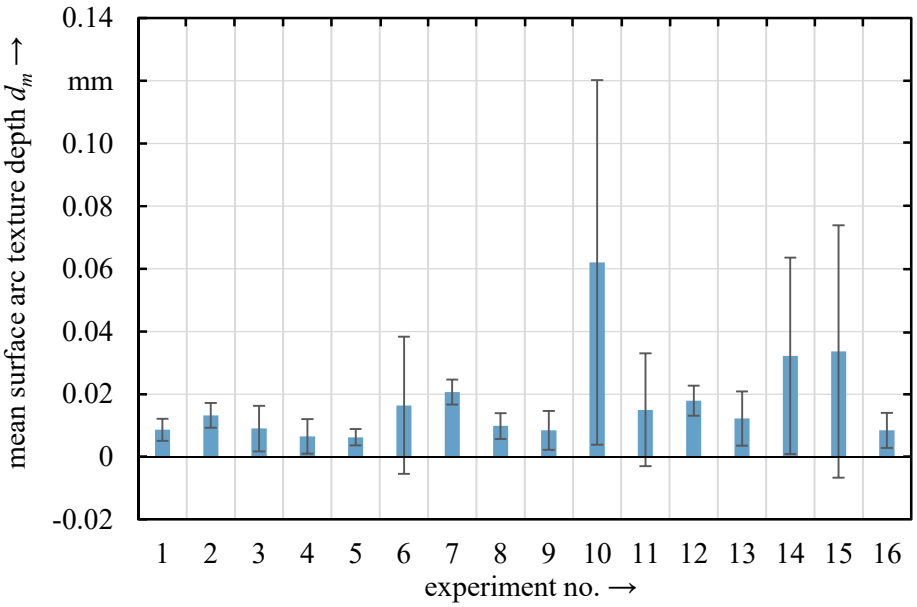

Figure 11. Mean surface arc texture depth (d_m) and its standard deviation (S_d).

By using a MATLAB code, the local minima and maxima along the weld seam surface were identified and the height difference of every local minimum and the following local maximum was calculated. Then, for the evaluation of the regularity of the arc formation, the standard deviation of the arc texture depth was calculated for the 16 experiments conducted in study 1. The results can be seen in figure 11. In experiment no. 5, the standard deviation of the arc depth was the lowest with 0.0026 mm.

Additionally, the numbers of local minima and maxima were counted in the evaluation of the weld seam arc texture (see the numeration in figure 10). The evaluation of the arc texture clarified that the measured number n_{meas} of local minima and maxima derived from the point cloud deviated from the theoretical number $n_{theoret}$ of arcs for some conducted experiments. The theoretical number $n_{theoret}$ of arcs results from the ratio of the rotational speed n to the welding speed v_s, multiplied by the length l of the evaluated distance of the weld seam, which was 50 mm:

$$n_{theoret} = \frac{n}{v_s} \cdot l \,. \tag{2}$$

It should be noted that n_{meas} depends on the accuracy of the measurement. Information about the profilometer used in this paper is given in section 2.3.3. By evaluating the ratio r_{arc} between the amount of measured arc numbers n_{meas} to the amount of theoretical arc numbers $n_{theoret}$, a statement can be made about the correct setting of the parameters rotational speed n and welding speed v_s:

$$r_{arc} = \frac{n_{meas}}{n_{theoret}} \,. \tag{3}$$

If the ratio r_{arc} was significantly below 1, the n/v_s ratio was too high and vice versa. This is also shown by the trendline depicted in figure 12. Remarkably, the experiment with the best welding result after the visual inspection (no. 1) is almost exactly at the intersection between the trendline and the ideal ratio, which is 1. The closer the experiments in figure 12 were to the intersection of the two lines, the better the surface quality of the weld seam was.

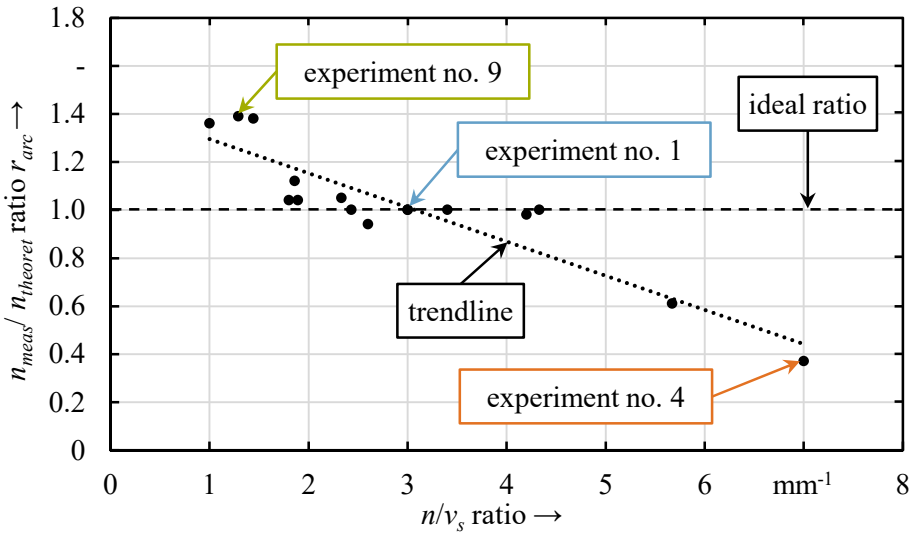

Figure 12. Ratio of the measured and the theoretical number of surface arcs r_{arc} as a function of the n/v_s ratio of the experiments conducted in study 1.

Figure 13 compares the surface profiles of longitudinal sections of experiments no. 1 (ideal r_{arc}), 4 (lowest r_{arc}), and 9 (highest r_{arc}). Evidently, experiment no. 1 had a very regular surface arc texture. Both the periodicity of the arc texture and the depth of the single arc textures are more regular than in the other two tests illustrated in figure 13.

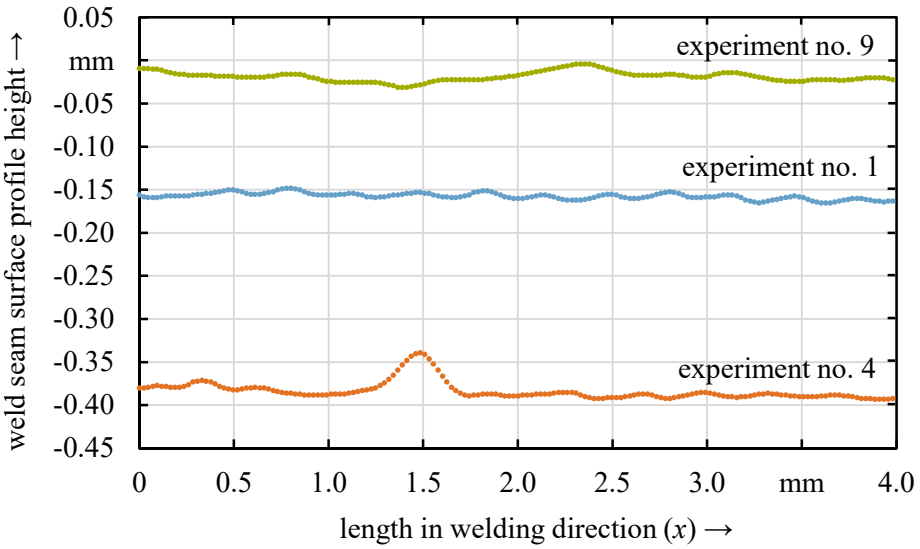

Figure 13. Comparison of the surface profile heights along the centerline (C) between experiments no. 1, 4 and 9.

Furthermore, the topography signals along the centerline (C) were subjected to a Fast Fourier Transformation (FFT). The ideal welding result would show a perfect sinusoidal surface profile and thus only the frequency f_1 in the frequency spectrum. Thereby the frequency f_1 corresponds to the n/v_s ratio.

The results of the FFT for experiments no. 1, 4, and 9 are given in figure 14. In all experiments from study 1, with the exception of experiment no. 4, pronounced spectral components occurred for the frequency f_1. The n/v_s ratio was 3 in experiment no. 1, 7 in experiment no. 4, and 1.3 in experiment no. 9 (see figure 3). In some experiments the surface profile also contained remarkable spectral components with the double frequency f_2 and in experiment no. 1 even with the triple frequency f_3 of the n/v_s ratio. Additionally, pronounced amplitudes outside the frequency f_1 and their integer multiples occurred for some experiments.

Experiment no. 1, which showed the highest quality after the visual inspection, evinced the greatest similarity with a perfect sinusoidal oscillation. The frequency spectrum in figure 14 (a) is dominated by the frequency f_1. The higher the n/v_s ratios of the experiments were, the lower were the profile components of the frequencies f_1, f_2, and f_3. In experiment no. 4, f_1 even showed no pronounced amplitude at all for f_1, f_2, and f_3. This is due to the fact that the surface arc texture characteristic decreases with higher n/v_s ratios. At experiments with lower n/v_s ratios, the noise between the frequencies f_1 and its integer multiples increased. Stochastically distributed irregularities occurred over the entire frequency spectrum. This can also be seen in the frequency spectrum of experiment no. 9 in figure 14 (c). Consequently, the frequency spectrum of the surface arc texture can also be suitable for the evaluation of the surface regularity of friction stir welds. The closer the surface arc texture of the friction stir weld comes to the ideal sinusoidal profile, the better the surface quality.

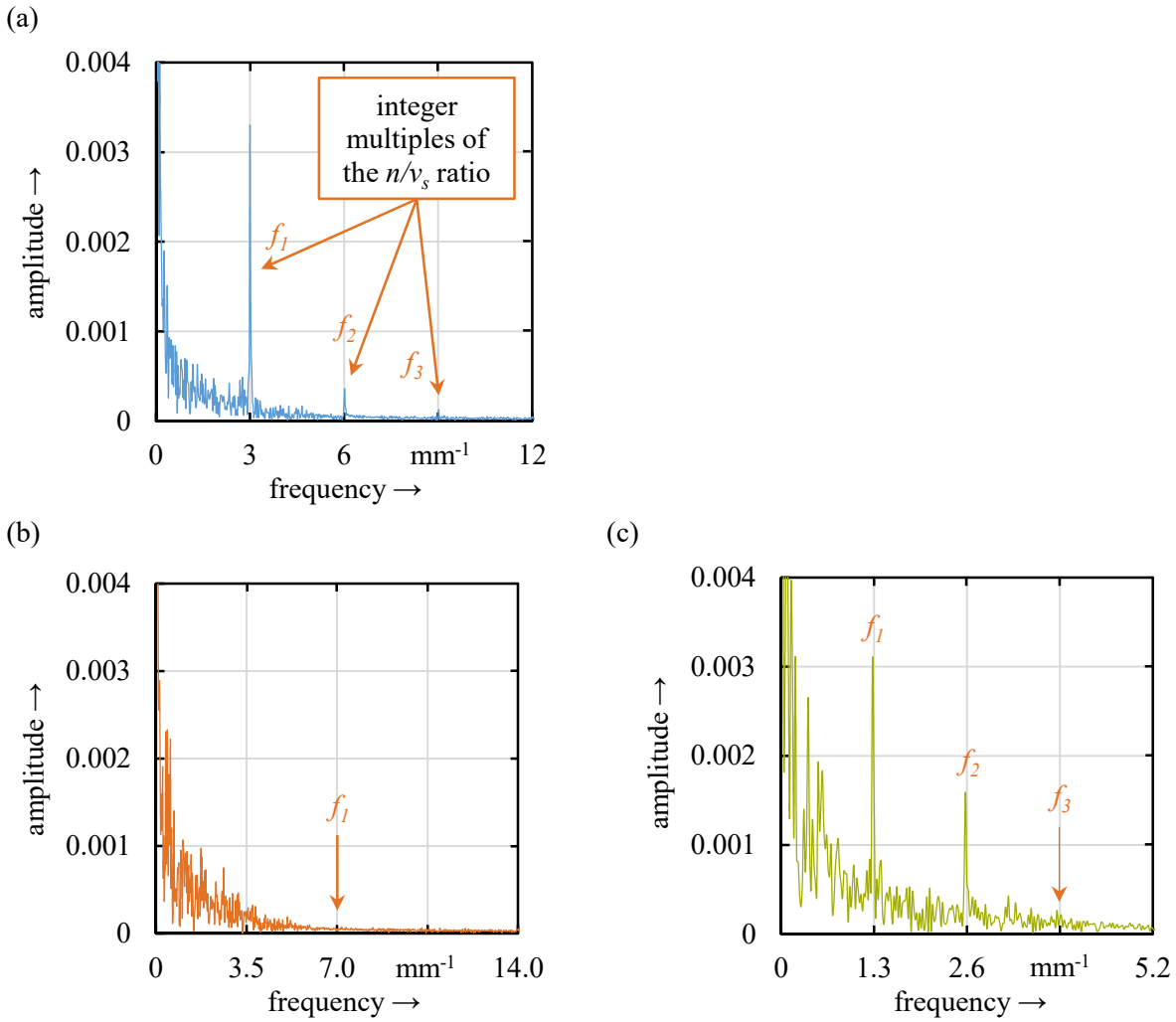

Figure 14. Frequency spectra of the surface topographies along the centerline (C) for experiment no. 1 (a), experiment no. 4 (b), and experiment no. 9 (c).

3.2.4. Surface lack of fill. The surface lack of fill (surface LOF) occurred exclusively in study 2 using the welding tool with spiral shoulder contour. Figure 15 illustrates the surface height profile of a cross section from experiment no. 22. Thereby, the crack on the surface is clearly visible.

The surface lack of fill can be identified by evaluating the standard deviation of the minima of the cross section profiles because of the very irregular depth of the crack. If the standard deviation of the profile minima Sp,min along the welding direction is small, this indicates a weld seam without surface lack of fill. A high standard deviation of the profile's minima indicates a crack or seam collapse in the seam surface. Figure 16 shows the standard deviations of the profile minima Sp,min along the evaluated 50 mm section (area (A) in figure 2) for each experiment.

Figure 17 demonstrates sections of the experiments no. 19, 25 and 32. In experiment no. 19 no surface LOF has occurred. In experiments no. 25 and 32 the surface lack of fill is clearly visible.

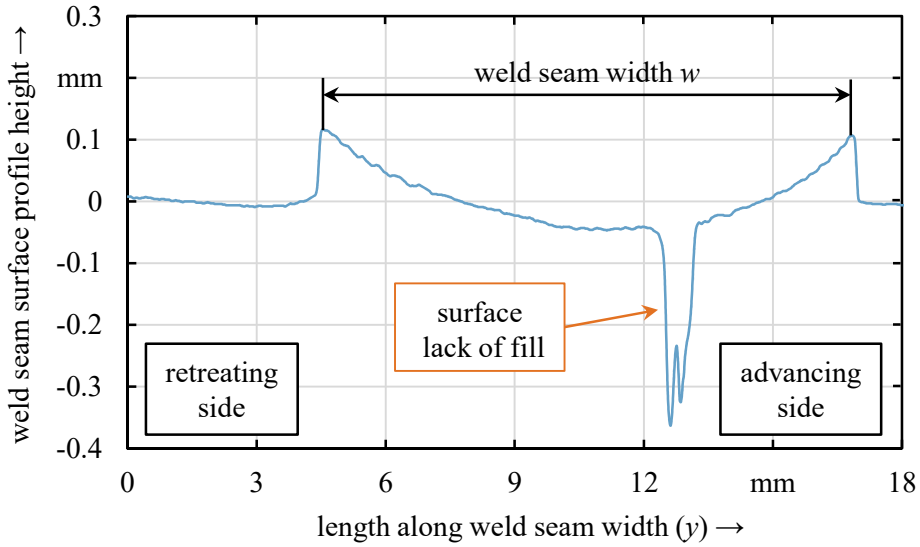

Figure 15. Surface profile height from experiment no. 22 with occurring surface lack of fill.

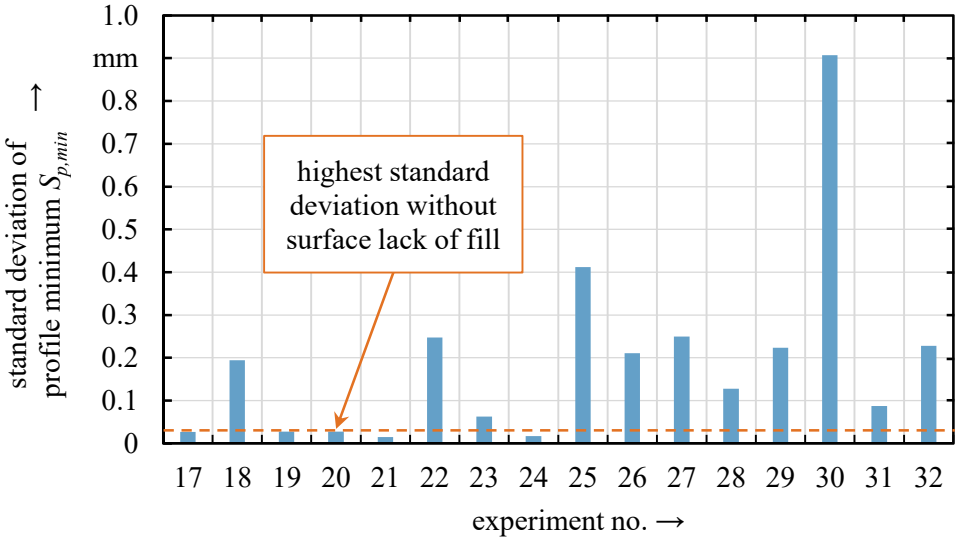

Figure 16. Standard deviations of the profile minima ($S_{p,min}$) for study 2.

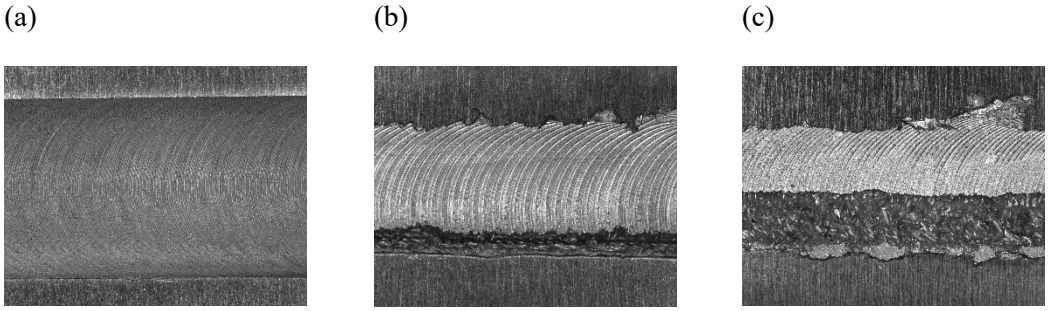

Figure 17. (a) Exp. no. 19; (b) Exp. no. 25; (c) Exp. no. 32.

3.2.5. Irregular weld seam width. The width of some welds produced in study 2 was very irregular. To evaluate the weld seam width, the y-coordinates of the profile height maxima on the retreating side max_{RS} and on the advancing side max_{AS} were determined for each cross section of the weld in question. The difference of the two determined y-coordinates was defined as the weld seam width w (see figure 15):

$$w = max_{AS} - max_{RS} . \quad (4)$$

In order to evaluate the uniformity of the weld seam width w, the standard deviation along the evaluated 50 mm section of the weld seam was used. Figure 18 shows the mean weld seam width w_m and the standard deviations of the weld seam width S_w from study 2.

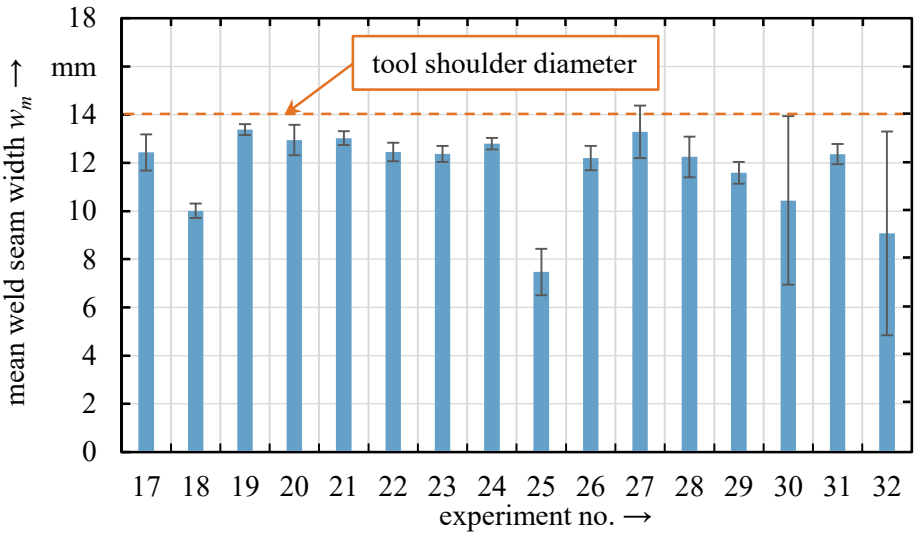

Figure 18. Mean weld seam width (w_m) and its standard deviation (S_w).

Figure 17 illustrates pictures of the experiments no. 19, 25 and 32. In experiment no. 19, the standard deviation S_w of the weld width w was the smallest and thus the weld width the most regular. Experiment no. 25 showed the smallest mean weld seam width w_m and experiment no. 32 the largest S_w and thus the largest irregularity in the weld seam width.

4. Conclusions and future work

The aim of this work was to derive one-dimensional indicators from the surface topography of friction stir welds, which enable the detection and quantification of surface defects and features. For this purpose, two test series with two different shoulder geometries were performed. The resulting welds were inspected visually and the surface topography was recorded using structured light projection. Key indicators were derived from the resulting three-dimensional point cloud to describe the surface defects and characteristics that occurred. The key figures determined are summarized in table 1. With the help of the key indicators listed in table 2, frequently occurring surface defects in friction stir welds can be detected and quantified.

The subject of future investigations will be the transfer of the knowledge gained in this work to inline applications. The goal is to control the process parameters in order to optimize the weld surface and thus to increase the weld quality.

Table 2. Summary of the determined key indicators to describe the surface defects and properties at FSW by means of structured light projection.

Surface defect	**Key indicator 1**	**Key indicator 2**
Flash formation	Maximum flash height f_{max}	Standard deviation of the flash height S_f
Surface galling	Peak material volume V_{mp}	n/a
Irregular arc texture formation	Standard deviation of the arc texture depth S_d	Ratio of the measured and the theoretical number of surface arcs r_{arc}
Surface LOF	Standard deviation of the profile minima $S_{p,min}$	n/a
Irregular weld seam width	Standard deviation of the weld seam width S_w	n/a

Acknowledgments
The IGF-research project no. 19389 N of the "Research Association on Welding and Allied Processes of the DVS" has been funded by the AiF within the framework for the promotion of industrial community research (IGF) of the Federal Ministry for Economic Affairs and Energy because of a decision of the German Bundestag.

References

[1] U.S. Geological Survey 1995 - 2018 Mineral Commodity Summaries *U.S. Department of the Interior, U.S. Geological Survey* (*USGS*)
[2] Askeland D R 1996 *Materialwissenschaften* ('Material sciences') (Heidelberg: Springer Spektrum)
[3] Colligan K J 2010 The friction stir welding process: an overview Lohwasser D and Chen Z Friction stir welding - From basics to applications 15–41
[4] Kallee S W 2010 Industrial applications of friction stir welding Lohwasser D and Chen Z Friction stir welding - From basics to applications 118–163
[5] Kahnert M, Mestek M, Windisch M, Tessier I and Okualla M 2012 Preparation of Friction Stir Welding of the Aluminum Alloy AA 2219 for Launcher Applications *9th International Friction Stir Welding Symposium* (Huntsville, Alabama) May 15th – 17th 2012
[6] Soni N, Chandrashekhar S, Kumar A and Chary V R 2017 Defects Formation during Friction Stir Welding: A Review *International Journal of Engineering and Management Research* **Volume-7, Issue-3** 121–125
[7] DIN Deutsches Institut für Normung e. V. DIN EN ISO **25239-5:2011** Rührreibschweißen – Aluminium – part 5: Qualitäts- und Prüfungsanforderungen (Berlin: Beuth Verlag GmbH)
[8] DIN Deutsches Institut für Normung e. V. DIN EN ISO **25239-4:2011** Rührreibschweißen – Aluminium – part 4: Anforderung und Qualifizierung von Schweißverfahren (Berlin: Beuth Verlag GmbH)

[9] Zettler R, Vugrin T and Schmuecker M 2010 Effects and defects of friction stir welds Lohwasser D and Chen Z Friction stir welding - From basics to applications 245–276
[10] Bachmann A, Gamper J, Krutzlinger M, Zens A and Zaeh M F 2017 Adaptive model-based temperature control in friction stir welding *Int J Adv Manuf Technol* **93** 1157–1171
[11] Sinha P, Muthukumaran S, Sivakumar R and Mukherjee S K 2008 Condition monitoring of first mode of metal transfer in friction stir welding by image processing techniques *Int J Adv Manuf Technol* **36** 484–489
[12] Ranjan R, Khan A R, Parikh C, Jain R, Mahto R P, Pal S, Pal S K and Chakravarty D 2016 Classification and identification of surface defects in friction stir welding: An image processing approach *Journal of Manufacturing Processes* **22** 237–253
[13] Deng Y, Zuo D and Song B 2014 Analysis of the main factors affecting the surface morphology of FSJ joint *Advanced Materials Research* **1027** 183–186
[14] Zuo L, Zuo D, Zhu Y and Wang H 2018 Effect of process parameters on surface topography of friction stir welding *Int J Adv Manuf Technol*
[15] Bachmann A, Krutzlinger M and Zaeh M F 2018 Influence of the welding temperature and the welding speed on the mechanical properties of friction stir welds in EN AW-2219-T87 *IOP Conf. Ser.: Mater. Sci. Eng.* **373** 1–14
[16] Zaeh M F, Gebhard P, Roos E, Noveva R, Kraetschmer D and Kleih L 2010 Eignung von Anlagen für das Rührreibschweißen und Übertragbarkeit von Schweißparametern ('Suitability of equipment for friction stir welding and transferability of welding parameters') *Düsseldorf* vol. 267 ed Deutscher Verband für Schweißen und verwandte Verfahren e. V. DVS-Berichte (Düsseldorf: DVS Media GmbH 410–416
[17] Federation of European Producers of Abrasives (FEPA) **43-2:2017** Grains of fused aluminium oxide, silicon carbide and other abrasive materials for coated abrasives Microgrits P 240 to P 5000
[18] Petzow G 2015 *Metallographisches, keramographisches, plastographisches Ätzen* ('Metallographic, ceramographic, plastographic etching') (Stuttgart: Gebrüder Borntraeger)
[19] Stachowiak G and Batchelor A 2005 *Engineering Tribology* (Oxford: Butterworth-Heinemann)
[20] DIN Deutsches Institut für Normung e. V. DIN EN ISO **25178-2:2012** Geometrische Produktspezifikation (GPS) - Oberflächenbeschaffenheit: Flächenhaft – part 2: Begriffe und Oberflächen-Kenngrößen (Berlin: Beuth Verlag GmbH)
[21] DIN Deutsches Institut für Normung e. V. DIN EN ISO **25178-3:2012** Geometrische Produktspezifikation (GPS) - Oberflächenbeschaffenheit: Flächenhaft – part 3: Spezifikationsoperatoren (Berlin: Beuth Verlag GmbH)